The Astrophysical Journal, 909:95 (11pp), 2021 March 1 https://doi.org/10.3847/1538-4357/abd4e6

Switchbacks Explained: Super-Parker Fields—The Other Side of the Sub-Parker Spiral

N. A. Schwadron[1,2] and D. J. McComas[2]
[1] University of New Hampshire, Durham, NH 03824, USA
[2] Department of Astrophysical Sciences, Princeton University, Princeton, NJ 08544, USA
Received 2020 November 4; revised 2020 December 6; accepted 2020 December 16; published 2021 March 9

Abstract

We provide a simple geometric explanation for the source of switchbacks and associated large and one-sided transverse flows in the solar wind observed by the Parker Solar Probe (PSP). The more radial, sub-Parker spiral structure of the heliospheric magnetic field observed previously by Ulysses, ACE, and STEREO is created within rarefaction regions where footpoint motion from the source of fast into slow wind at the Sun creates a magnetic fieldline connection across solar wind speed shear. Conversely, when footpoints move from the source of slow wind into faster wind, a super-Parker spiral field structure is formed: below the Alfvén critical point, one-sided transverse field-aligned flows develop; above the Alfvén critical point, the field structure contracts between adjacent solar wind flows, and the radial field component decreases in magnitude with distance from the Sun, eventually reversing into a switchback. The sub-Parker and super-Parker spirals behave functionally as opposites. Observations from PSP confirm the paucity of switchbacks within rarefaction regions and immediately outside these rarefaction regions, we observe numerous switchbacks in the magnetic field that are directly associated with abrupt transients in solar wind speed. The magnetic field strength, the radial component of the magnetic field, the speed gradients, radial Alfvén speed, and the ratio of the sound speed to the radial Alfvén speed all conform to predictions based on the sub-Parker and super-Parker spirals within rarefaction regions and solar wind speed enhancements (spikes or jets), respectively. Critically, the predictions associated with the super-Parker spiral naturally explain the observations of switchbacks being associated with unexpectedly large and one-sided tangential flows.

Unified Astronomy Thesaurus concepts: Active solar corona (1988); Solar wind (1534); Solar coronal waves (1995); Solar coronal loops (1485); Solar coronal holes (1484); Solar coronal plumes (2039); Solar magnetic fields (1503); Interplanetary magnetic fields (824); Solar spicules (1525)

1. Introduction

The solar wind rapidly accelerates in the corona at ~2–5 R_s and then becomes super-Alfvénic at ~10–20 R_s (Katsikas et al. 2010; Goelzer et al. 2014). It is this latter transition where the solar wind ram pressure becomes dominant, overcoming both the magnetic and thermal pressure. The processes that transfer energy and dissipate this energy to heat the corona and power the solar wind remain critical questions in heliophysics and astrophysics, and are at the heart of the scientific motivations for the Parker Solar Probe (PSP; McComas et al. 2007; Fox et al. 2016).

On PSP, the solar wind is observed by the Solar Wind Electrons Alphas and Protons Investigation (SWEAP; Kasper et al. 2016) and the magnetic field by the Electromagnetic Fields Investigation (FIELDS; Bale et al. 2016). The Integrated Science Investigation of the Sun (IS⊙IS) instrument suite (McComas et al. 2016) provides comprehensive measurements of energetic particles over the range 0.02–200 MeV nucleon^{-1}.

PSP observes thousands of intervals (duration from seconds to tens of minutes) where the speed of the solar wind flow suddenly jumps and includes a large, one-sided transverse flow, while simultaneously the magnetic field orientation rotates through large angles, before returning to roughly the prior solar wind conditions. The observed switchbacks (radial magnetic field reversals) are associated with the change in magnetic field direction and velocity spikes associated with the sharp increase in solar wind speed (Bale et al. 2019; Kasper et al. 2019; de Wit et al. 2020; Horbury et al. 2020; Mozer et al. 2020; Rouillard et al. 2020; Tenerani et al. 2020).

Magnetic switchbacks have been studied extensively in fast wind from coronal holes (e.g., Kahler et al. 1996) at 1 au, and beyond 1 au with Ulysses (e.g., Balogh et al. 1999; Yamauchi et al. 2004b; Neugebauer & Goldstein 2013). Observations of switchbacks have also been made inside 1 au with Helios (Borovsky 2016; Horbury et al. 2018) prior to the observations by PSP. Strong magnetic-field deviations from the Parker spiral are observed where there are local increases in the radial solar wind speed (Michel 1967), and associated with one-sided or pulsed Alfvénic fluctuations (Gosling et al. 2009, 2011). The one-sided nature of switchbacks is especially clear in PSP observations. Kasper et al. (2019) states that "Transients, including the Alfvénic jets, are one-sided, in that if the field rotates more than ~60°, then B_T is always positive and V_{pT} always exceeds 33 km s^{-1}." (Here, B_T is the tangential magnetic field component, and V_{pT} is the proton tangential component.)

The transverse flows observed by PSP far exceed those in the Weber–Davis model (Weber & Davis 1967) where the lower corona is taken to rotate rigidly at the mean rotational period of the Sun. To this point Kasper et al. (2019) state: "The large rotational velocities measured .. exceed the value in the axisymmetric Weber–Davis model, in which $V_{pT}(R_A) < 0.1\Omega_\odot R_A$, by more than an order of magnitude." Here, $\Omega_\odot$ refers to the solar rotation rate and R_A refers to the Alfvén radius. For an Alfvén point of 15 R_s, the $V_{pT}(R_A) < 3$ km s^{-1}. Thus, the one-sided transverse flows are a key observable from PSP that any switchback theory must also explain.

Table 1 summarizes these key observations from PSP related to switchbacks and tangential flows. This paper provides a

Table 1
PSP Observations of Switchbacks and Transverse Flows

Obs.	References
Switchbacked magnetic field	Kasper et al. (2019), Bale et al. (2019)
Transient jets or pulsations	Kasper et al. (2019)
One-sided tangential flows	Kasper et al. (2019)
Large transverse, co-rotational flows	Kasper et al. (2019)
Alfvénic correlation $\delta \boldsymbol{v}$ to $\delta \boldsymbol{B}$	Bale et al. (2019)
Anti-correlated plasma density n_e and $\lvert \boldsymbol{B} \rvert$	Bale et al. (2019)

simple and natural geometric explanation for all of these apparently disparate observations that unifies the interpretation of switchbacks and the transverse flows observed by PSP.

There are already a variety of models and conjectures to explain various (although not all) aspects of switchbacks. One example relates to nonlinear shear driven turbulence (Ruffolo et al. 2020). In the presence of large speed gradients within the solar wind, there are a number of important effects that should be considered. As already indicated, the situation where faster wind outruns slower wind leads to the formation of rarefaction regions. However, if speed gradients exist across magnetic flux tubes, the effects of nonlinear shear driven turbulence can result in switchbacks in the magnetic field (Ruffolo et al. 2020). Prior remote observations (DeForest et al. 2016) show a transition from striated solar coronal structures to more isotropic "flocculated" fluctuations in the transition just outside the Alfvén critical point. This transition in the geometry of solar wind structures is powered by the relative velocities of adjacent coronal magnetic flux tubes.

Another conjecture relates to the effects of interchange reconnection (ICX) on the magnetic structure of the solar wind. Fisk & Kasper (2020) argue that the large transverse flows observed by PSP are a result of transverse flows in the corona and are part of a closed global circulation pattern of magnetic flux open to the solar wind. The circulation pattern at the Sun is sustained by the combined effects of differential motion and ICX (Fisk & Schwadron 2001). Zank et al. (2020) develop an evolution equation for the development of switchbacks resulting from ICX between coronal loops and the open magnetic field. Results from the model include complex aggregated groups of switchbacks and an example event from the model resembles PSP observations.

The concept of ICX was developed by Crooker et al. (2002) to explain how magnetic flux injected by coronal mass ejections can be reduced without disconnecting magnetic fields entirely. Coronal mass ejections (CMEs) originate in closed magnetic field structures and add magnetic flux to the heliosphere as they move away from the Sun. Observations of ejecta in the solar wind show signatures including counter-streaming suprathermal electrons that show outflowing electron heat flux moving in both directions along closed field lines (e.g., Gosling et al. 1987). These observations confirm the addition of magnetic flux from ejecta, and show that without changing the magnetic topology of CME ejecta, the total flux in the heliosphere would continue to increase, which leads to a "magnetic field magnitude catastrophe" (Gosling 1975; McComas 1995). Disconnection was pictured as magnetic reconnection between magnetic field lines to create U-shaped structures that are disconnected entirely from the Sun and are then convected through the heliosphere by the solar wind (McComas et al. 1991). While disconnection is one possible solution to the magnetic field catastrophe, it was noted that signatures of heat flux dropouts (McComas et al. 1989) should be associated with disconnection. However, the number of heat flux dropouts observed were found to be at least a factor of four too small to account for the loss of magnetic flux from that added by coronal mass ejections (McComas et al. 1992). Crooker et al. (2002) suggested that the primary flux balancing mechanism is instead from ICX associated with magnetic reconnection between closed fields from coronal mass ejecta and open magnetic fields in the surrounding solar wind. ICX was considered as way for open magnetic field lines to reconnect with loops in the corona, and thereby enable large-scale redistribution of open magnetic fields beyond coronal-hole boundaries (Fisk et al. 1999; Fisk & Schwadron 2001).

The conjecture that footpoint motion is driven by differential motion in coronal holes and ICX beyond coronal holes was made previously by Fisk et al. (1999) and Fisk & Schwadron (2001). The basis of this conjecture is rooted in the difference between coronal holes and the surrounding source regions of solar wind, which remains an area of active research. Potential field models that approximate the corona as having zero current below the source surface radius (~3 solar radii) show that open magnetic flux originates predominantly from coronal holes (Schatten et al. 1969). Footpoint motions are driven by the Sun's differential motion and therefore convect open magnetic field lines continually across coronal-hole boundaries (Fisk et al. 1999; Fisk & Schwadron 2001; Schwadron 2002). Outside coronal holes, ICX between open magnetic field lines and large loops may continue to facilitate the motion of the open magnetic field footpoints. The support for this view of footpoint motion is rooted in remote solar observations:

1. The photosphere rotates differentially (e.g., Snodgrass 1983);
2. Coronal holes tend to rotate rigidly with the Sun, at approximately the equatorial rotation rate (e.g., Bird & Edenhofer 1990).

In this picture, coronal holes represent the boundary where there is a transition between the open magnetic flux concentrated within the coronal hole and the more distributed open magnetic flux that moves through differential rotation and ICX beyond the coronal hole.

This picture of the Sun's open magnetic field has remained difficult to verify observationally. One observational signature of footpoint motion was found in rarefaction regions where the magnetic field line is stretched between faster solar wind that streams out ahead of slower wind (Murphy et al. 2002; Schwadron 2002), leading to the formation of the sub-Parker spiral (Schwadron & McComas 2005; Schwadron et al. 2005). Note that rarefaction regions are formed where faster solar wind outruns slower solar wind, and these structures are characterized by an almost monotonic decrease in the speed of solar wind. Rarefaction regions often map back to regions with small longitudinal extents on the Sun, termed "dwells" (Schwenn 1990). Because stream interfaces typically co-rotate with the Sun, co-rotating rarefaction regions are formed from the trailing edge of coronal holes (Smith et al. 2000).

Without footpoint motion, magnetic field lines are not connected between faster and slower wind, and conform to Parker spirals associated with their various solar wind speeds.

In contrast, the straightening of the magnetic field in the rarefaction region due to footpoint motion at the Sun creates a magnetic field structure with a larger radial component than the Parker spiral magnetic field. The deviations in field direction are extremely prominent and commonly observed by Ulysses in co-rotating rarefaction regions (Murphy et al. 2002; Schwadron & McComas 2005; Schwadron et al. 2005). The magnetic structure in rarefaction regions is referred to as the *sub-Parker spiral* (Schwadron & McComas 2005; Schwadron et al. 2005) as it is less tightly wound than would be expected for the observed solar wind speed. Another interpretation (Gosling & Skoug 2002) associated radial magnetic fields with abrupt temporal changes in the solar wind: the "radially directed kink in the magnetic field connects the different spirals associated with the faster and slower flows immediately preceding and following the temporal flow speed discontinuity." This description is appropriate prior to or without the development of a rarefaction region.

In this paper, we show that the sub-Parker spiral depends on the direction of footpoint motion relative to the gradient between fast and slow solar wind. If the direction of footpoint motion is reversed with respect to the solar wind speed gradient, a different and distinct magnetic field structure is produced in which the fieldline connection between fast and slow wind contracts and ultimately reverses the magnetic field, producing a switchback. We begin by conceptually describing the super-Parker spiral and its obvious extension to switchbacks as super-Parker spirals in Section 2. In Section 3, we use observations from SWEAP and FIELDS to test for the presence of the sub-Parker spiral, and the super-Parker field structures. We report observations from several rarefaction regions and in nearby intervals of switchbacked fields and compare them to a simple quantitative model for such magnetic structures (see Appendix). Finally, in Section 4 we discuss the implications of this new interpretation and bring closure on the fundamental source for magnetic switchbacks and their uniquely one-sided transverse flows.

2. From Sub-Parker to Super-Parker Spirals

The concept of the sub-Parker spiral is illustrated in Figure 1 (top panel). Near the Sun, footpoint motion from the source of coronal-hole associated fast wind into slow wind creates a magnetic fieldline connection across the interface between fast and slow solar wind. The fast solar wind draws the magnetic field out more quickly than the slow solar wind, therefore forming a rarefaction region. The magnetic field, stretched between faster solar wind flow and slower solar wind becomes increasingly radial with distance from the Sun. The basic prediction in this case is the association between rarefaction and the sub-Parker spiral magnetic field, which has a stronger radial component than the Parker spiral. A recent study by Schwadron et al. (2020) shows that the sub-Parker spiral provides relatively short fieldline connections from the PSP spacecraft to the compressions and shocks surrounding co-rotating interaction regions in the inner heliosphere (at ~0.7–10 au). These shorter fieldline connections are essential in explaining the persistence of energetic particles from ~100 keV to > MeV observed by IS⊙IS up to ~1 week after the passage of a stream interface.

The opposite configuration or super-Parker spiral is illustrated in the bottom panel of Figure 1. The fundamental difference between the sub-Parker spiral and the super-Parker

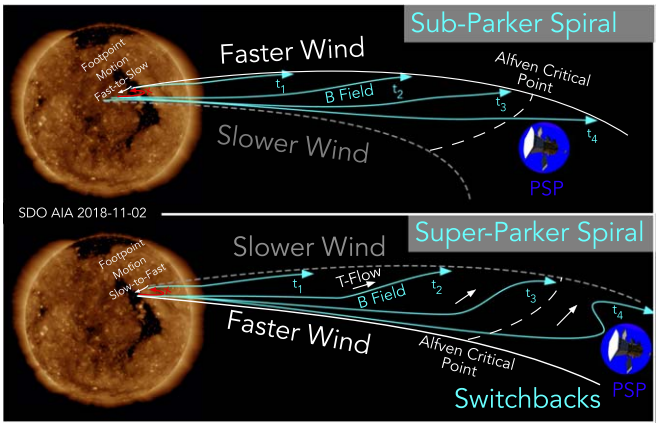

Figure 1. The sub-Parker spiral (top panel) and the super-Parker spiral (bottom panel) result from footpoint motion between source regions of fast and slow solar wind. In the case of the sub-Parker spiral, footpoint motion from the source of fast-to-slow wind creates a fieldline connection that gets straightened as fast wind drags out magnetic field lines more quickly than the slow wind. The sub-Parker spiral is associated with magnetic field lines with larger radial components than the Parker spiral. When footpoint motion is reversed (bottom panel), and footpoints move from the source of slow into fast wind, then the wind shear kinks the magnetic field. In this case, the faster wind moves along the magnetic field below the Alfvén critical point, forming compressions and tangential flows and develops into a switchback above the Alfvén critical point.

spiral is the direction of footpoint motion. In the case of the super-Parker spiral, footpoints move from the source of slow wind into faster wind. Below the Alfvén critical point, the plasma flows along the magnetic field, and magnetic field tension resists the growth of fieldline curvature. Therefore, faster wind overtakes slower wind below the Alfvén critical point, forming plasma compression and transverse flow along the field.

Above the Alfvén critical point, the solar wind ram pressure overwhelms magnetic fieldline tension. The shear between faster and slower solar wind perturbs the structure in the magnetic field and the faster flow in the solar wind drags out the magnetic field, overtaking adjacent regions of slower solar wind. The fieldline connection from slower to faster wind therefore eventually creates radial inversions, or switchbacks, in the magnetic field.

The motion of footpoints in Figure 1 is driven in part by differential motion and is mediated by ICX across the opposite edges of the coronal hole or other regions with speed shear. The sense of footpoint motion is largely in the direction opposite of the sense of equatorial rotation since it is driven by differential motion. This directionality of footpoint motion in the super-Parker spiral creates tangential flows in the direction of co-rotation as observed by PSP (Kasper et al. 2019).

In this picture, the orientation of tangential flows is linked to the direction of footpoint motion at the Sun driven by differential motion, as detailed in the Introduction. The fact that coronal holes tend to rotate rigidly implies that differential motions in the photosphere drive open magnetic field footpoints into coronal holes on their leading edge (leading with respect to rigid rotation), and out of coronal holes on their trailing edge. Thus, this sense of footpoint motion consistently connects slower wind from outside the coronal hole with faster wind from within the coronal hole in the opposite sense on the leading and trailing edges of a coronal hole.

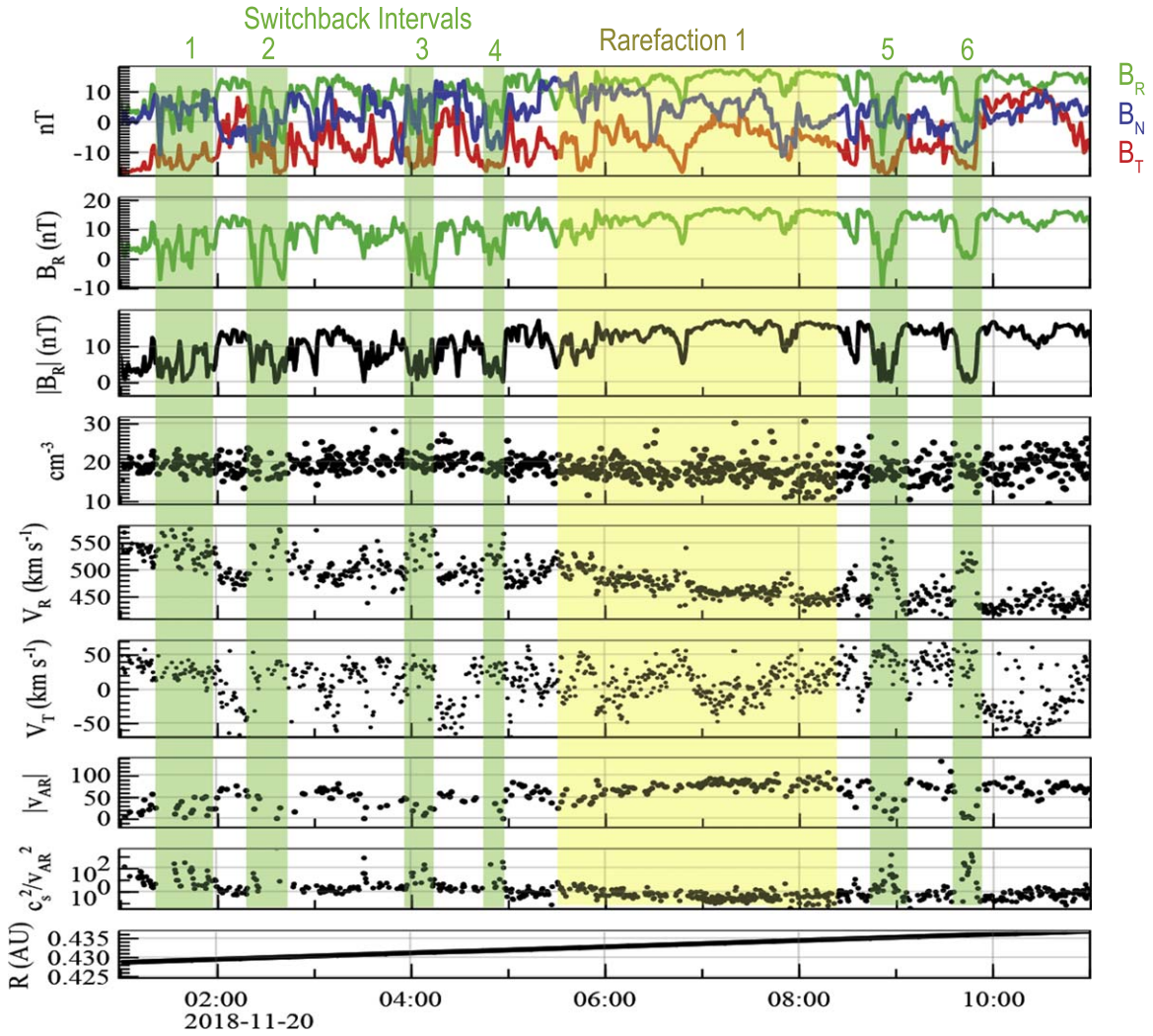

Figure 2. Observations from PSP: FIELDS data (panels 1–3), and SWEAP data (panels 4, 5) on 2018 November 20. In panels 6, and 7 we form the radial Alfvén speed and the ratio of the sound speed to the radial Alfvén speed from the SWEAP and FIELDS observations. Radial distance from the Sun is shown in the bottom panel. Green shaded regions show intervals where switchbacks are observed. The yellow shaded region shows a rarefaction region.

3. PSP Observations of Rarefaction Regions and Switchbacks

We re-examine some PSP observations from Orbit 1 to test the prediction that switchbacks occur far less often in rarefaction regions. Observations from 2018 November 20 and 21 are shown in Figures 2 and 3, respectively. Within these observational periods, we identify two rarefaction regions as relatively steady, multi-hour periods of decreasing radial solar wind speed. Within rarefactions it is important to separate the underlying trend of a reduction in radial wind speed from small speed fluctuations ($<50\,\mathrm{km\,s^{-1}}$) occurring over short (<10 minutes) periods. In a similar vein, we identify 11 switchback intervals as periods larger than $\sim$10 minutes where the radial field component vanishes or switches sign. Note that switchback intervals often include many subintervals where the radial field may switch sign or vanish intermittently.

The trends within rarefactions agree with the key features associated with the sub-Parker spiral:

1. The prediction that switchbacks should preferentially occur outside of rarefaction regions is clearly supported by the observations in Figures 2 and 3. The only weak possible exception is in the first rarefaction region on 2018 November 20 06:45 where we observe a reduction in radial field strength and the radial component of the magnetic field. However, even for this event, we observe a slight increase in the radial component of the solar wind speed, suggesting that there is a super-Parker structure associated with the speed jump embedded within the rarefaction region.
2. Since footpoints move from the source of fast wind to slow wind in the direction opposite of co-rotation, we predict a tangential flow component that is negative. However, ICX and potentially changes along the flow history may lead to intermittent increases in the tangential flow component. Because the rarefaction region expands between faster and slower flow, any variations in the tangential flow will be accentuated. We therefore predicted a mix of positive and negative tangential flows, which is observed in both rarefaction regions.
3. We observe an increase in the radial magnetic field in both rarefaction regions. The second rarefaction region is more developed than the first, due to the larger and longer duration drop in speed through the rarefaction, and possibly the slightly larger distance from the Sun. In this

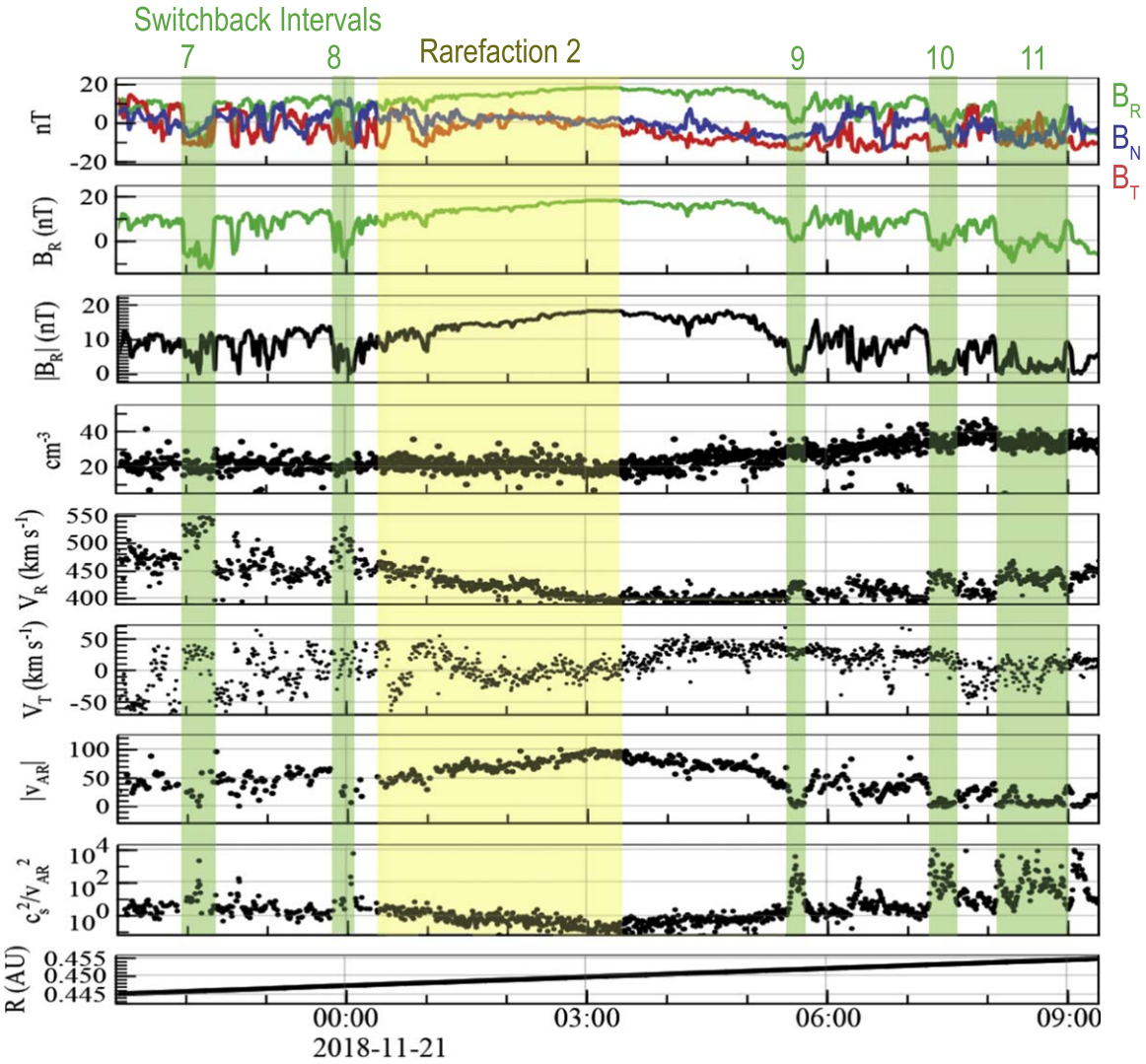

Figure 3. Observations from PSP: FIELDS data (panels 1–3), and SWEAP data (panels 4, 5) on 2018 November 21. The format is identical to Figure 3.

second rarefaction, the large increase in the radial magnetic field strength relative to the other two field components is particularly evident. This strongly supports the example calculation detailed in Appendix that the magnetic field within the sub-Parker spiral tends to make the field structure more radial than what would be observed in a Parker spiral.

4. This observation also directly supports the concept that the magnetic field is connected between faster and slower solar wind flow, contrary to the assumption of no footpoint motion associated with the Parker spiral magnetic fields.
5. The increase in radial magnetic field strength within the sub-Parker spiral should increase the radial Alfvén speed[3] magnitude and reduce the ratio of the sound speed to the radial Alfvén speed. Both of these effects are observed in each rarefaction region.

The trends (rows 3–13 in Table 2) observed where there are increases or jumps in solar wind speed counter those within rarefactions, and agree with the super-Parker spiral predictions in Appendix:

1. Switchbacks occur in regions where there are abrupt increases in solar wind speed, as opposed to the reduction in solar wind speed in rarefaction regions.
2. Tangential flows should be positive, in the direction of co-rotation, as discussed in the previous section.
3. The decrease in the radial magnetic field is evident in each of the regions identified.
4. There is a decrease in the radial magnetic field strength observed within each of the switchback field intervals. As shown in the Appendix, this trend supports the concept that the magnetic field contracts where the faster wind overtakes adjacent flow of slower solar wind.
5. The decrease in radial magnetic field strength within the super-Parker spiral decreases the radial Alfvén speed magnitude and increases the ratio of the sound speed to the radial Alfvén speed, which is consistently observed in ten of the eleven switchback regions observed.

PSP observations of magnetic and plasma structures show a number of common features as summarized in Table 2. Rows RF1 and RF2 apply to rarefaction regions, and rows SB1-SB11

[3] The radial Alfvén speed is defined, $v_{Ar} = B_r/\sqrt{4\pi\rho}$, where B_r is the radial magnetic field, and ρ is the mass density.

Table 2
PSP Observations within Rarefactions and Switchbacks

Event	Figures	$\lvert B_r\rvert$	B_r	V_r	V_t	$\lvert v_{Ar}\rvert$	$c_s^2/v_{Ar}^2\ \beta$	Sub-PS[a]	Super-PS[b]
RF-1[c]	2	↑	↑	↘	↑↓	↑	↓	6/6	0/6
RF-2[c]	3	↑	↑	↘	↓↑	↑	↓	6/6	0/6
SB-1[d]	2	↓	↓	↑	↑	↓	↑	0/6	6/6
SB-2[d]	2	↓	↓	↑	↑	↓	?	0/6	5/6
SB-3[d]	2	↓	↓	↑	↑	↓	↑	0/6	6/6
SB- 4[d]	2	↓	↓	↑	↑	↓	↑	0/6	6/6
SB-5[d]	2	↓	↓	↑	↑	↓	↑	0/6	6/6
SB-6[d]	2	↓	↓	↑	↑	↓	↑	0/6	6/6
SB-7[d]	3	↓	↓	↑	↑	↓	↑	0/6	6/6
SB-8[d]	3	↓	↓	↑	↑	↓	↑	0/6	6/6
SB-9[d]	3	↓	↓	↑	↑	↓	↑	0/6	6/6
SB-10[d]	3	↓	↓	↑	↑	↓	↑	0/6	6/6
SB-11[d]	3	↓	↓	↑	↑↓	↓	↑	1/6	5/6

Notes.
[a] Sub-Parker spiral—Sub-PS.
[b] Super-Parker spiral—Super-PS.
[c] Rarefaction—RF.
[d] Switchbacks—SB.

apply to intervals with switchbacks. The sub-Parker spiral should show enhanced radial magnetic field strength, an increased radial magnetic field component, a dropping radial solar wind speed, variable tangential flow, enhanced radial Alfvén speed magnitude, and reductions in the ratio of the sound speed to the radial Alfvén speed. In contrast, the super-Parker spiral should show the opposite trends including reduced radial magnetic field strength, decreased or reversed radial magnetic field component, an abrupt increase in radial solar wind speed, positive values for the tangential flow (flows in the direction of co-rotation), an abrupt decrease in the radial Alfvén speed magnitude, and abrupt increases in the ratio of the sound speed to the radial Alfvén speed. These predictions provide specific observational signatures, the presence of which are tested using PSP observations. The observational signatures are related analytically and are all important for identifying the presence of the sub-Parker spiral or the super-Parker spiral. Therefore, we use these observational signatures to "score" of each of the 13 intervals against all six criteria.

The last two columns of Table 2 provide this scoring. For both of the rarefactions studied, each of these 6 trends are observed, and the consistency with the sub-Parker spiral is six-for-six (column 8 in Table 2). For the switchback intervals, we find perfect agreement between predicted and observed behaviors for all but two of the intervals and even for those two switchbacks, the score was 5 out of 6. The only two exceptions include one case (switchback 2) resulting from missing or inconclusive data, and one case (switchback 11) where the tangential flows are not uniformly positive. This latter case however appears to have a more variable radial magnetic field and variable properties in general, suggesting that the interval includes an array of switchbacks embedded on smaller scales.

4. Conclusions

This study examines the development of magnetic structures in the solar wind observed by PSP. The sub-Parker spiral structure of the heliospheric magnetic field is created within rarefaction regions where footpoint motion at the Sun creates a magnetic fieldline connection across the gradient between fast and slow solar wind. As fast solar wind moves outward more quickly than slower solar wind, the magnetic structure across the rarefaction region becomes more radial than the Parker spiral. We have examined rarefaction regions observed by PSP and find they that are consistent with the sub-Parker structure.

The direction of footpoint motion at the Sun between the source of fast and slow wind is critical in defining the magnetic structure in the heliosphere. For situations in which magnetic field footpoints move from the source of fast wind into slow wind, the magnetic structure in the heliosphere is consistent with the sub-Parker spiral due to the expansion within the rarefaction region and the magnetic fieldline connection across it. In contrast, when footpoint motion is reversed from the source of slow wind into faster wind, the magnetic structure contracts between adjacent solar wind streams and forms into a super-Parker spiral as the solar wind moves out into the heliosphere. The radial component of the magnetic field decreases in magnitude with distance from the Sun and eventually reverses into a switchback.

The sub-Parker spiral and the super-Parker spiral behave functionally as opposites. The observations from PSP confirm the paucity of switchbacks within rarefaction regions. Immediately outside these rarefaction regions, we observe numerous intervals of switchbacks in the magnetic field that are directly associated with abrupt transients in solar wind speed. In contrast to the smooth monotonic speed transition within rarefaction regions, the switchbacks occur in "bursts." The clustering and plenitude of these bursts occurring in close proximity are consistent with PSP being magnetically connected to the leading edge of the coronal hole. The observations confirm the features of the sub-Parker spiral and the super-Parker spiral: the magnetic field strength, the radial component of the magnetic field, the speed gradients, tangential flows, Alfvén speed, and plasma beta all conform to predictions based on the sub-Parker and super-Parker spiral within rarefaction regions and solar wind speed enhancements (spikes or jets), respectively.

Table 3 describes key observations identified in the Introduction (Table 1) and how the super-Parker spiral accounts for these

Table 3
PSP Observations of Switchbacks and Transverse Flows Related the Super-Parker Spiral Magnetic Field

Observation	Mechanism
Switchbacked magnetic field	**Super-Parker spiral, fast flow overtakes adjacent slower flow above Alfvén critical point**
Transient jets or pulsations	Coronal holes, Interchange Reconnection[a], loop sources[b], plumes[c], spicules[d]
One-sided tangential flows	**Directional field-aligned flow below Alfvén critical point**
Transverse, co-rotational flows	**Differential motion drives footpoints counter to co-rotation**
Alfvénic correlation $\delta \boldsymbol{v}$ to $\delta \boldsymbol{B}$	Alfvénic wave development[e], Poynting flux from Alfvén wave energy source[f]
Anti-correlated n_e and $\lvert \boldsymbol{B}_r \rvert$	**Flow compression below Alfvén critical point**

Notes. Mechanisms in bold indicate new aspects introduced in this Paper.
[a] Fisk & Schwadron (2001), Fisk & Kasper (2020), Zank et al. (2020).
[b] Schwadron & McComas (2003), Fisk & Kasper (2020), Zank et al. (2020).
[c] Poletto (2015).
[d] Yamauchi et al. (2004a).
[e] Gosling et al. (2009), Kasper et al. (2019).
[f] Schwadron & McComas (2003).

observations. In the super-Parker spiral, the presence of footpoint motion at the Sun from the slow to fast wind source provides a configuration that leads to switchbacks as the faster wind overtakes adjacent slower wind flows. The source of faster flow can come from coronal holes, transients associated with ICX, loop sources, plumes, spicules or macro-scipules. These sources of solar wind variability have been noted as potential causes of transient jets or speed variations in the solar wind.

The one-sided, co-rotation-directed tangential flows observed by PSP has been one of the most important and baffling pieces of the puzzle. As shown in Figure 1, differential motion determines the orientation of tangential magnetic field variations, and the field-aligned flow below the Alfvén critical point. Tangential flow is thus oriented in the direction of co-rotation, naturally explaining the observed one-sided tangential flows. The field-aligned flow below the Alfvén critical point also causes the development of compressions, and explains the anti-correlation between density and magnetic field strength.

The Alfvénic correlation between velocity and field variations results from the development of Alfvénic structures in the solar wind. Beyond the Alfvén critical point, large-scale variations in the flow inevitably develop Alfvénic characteristics. Moreover, the ejection of magnetic field variations close to the Sun are consistent with Alfvénic structures (Schwadron & McComas 2003), as are the exhausts from magnetic reconnection. Therefore, whether the source involves Alfvén waves or ICX exhausts, an outcome is the development of Alfvénic variations with correlation between velocity and field deviations.

Thus, this paper reveals the origin for switchbacked magnetic field structures and one-sided tangential flows from the formation of the super-Parker spiral, the counterpart of the sub-Parker spiral. These magnetic structures are produced fundamentally through footpoint motion, respectively, into and out of coronal holes at the Sun caused by differential motion and ICX across regions with a strong gradient in solar wind speed. The existence of these field structures represents a significant departure from the standard Parker spiral, and naturally explains fundamental relationships between their solar wind source at the Sun and the magnetic and flow structures out in the heliosphere.

We are deeply indebted to everyone that helped make the Parker Solar Probe (PSP) mission possible. We thank the reviewer for their helpful comments and suggestions. We thank Dr. Stuart Bale for spotting an error in our initial plotting of the magnetic field. This work was supported as a part of the PSP mission under contract NNN06AA01C. Parker Solar Probe was designed, built, and is now operated by the Johns Hopkins Applied Physics Laboratory as part of NASA's Living with a Star (LWS) program (contract NNN06AA01C). Support from the LWS management and technical team has played a critical role in the success of the Parker Solar Probe mission.

Appendix
Sub-Parker and Super-Parker Spirals

In this appendix, we develop an analytical derivation that provides solutions for the sub-Parker and the super-Parker spiral. Schwadron et al. (2020) follow the ballistic propagation of plasma parcels from the Sun within the solar wind to determine the structure of the magnetic field in the inner heliosphere. Figure 4 shows the configuration near the Sun in the co-rotating reference frame along a boundary surface (at radius R_B) where footpoint motion moves magnetic footpoints between regions of faster wind (with speed $V + \delta V/2$) and regions of slower wind (with speed $V - \delta V/2$). The boundary surface is at a radius where the field has expanded and roughly reaches a uniform magnetic pressure. Footpoints rotate in the azimuthal direction at rate $\omega_\phi = -|\omega_\phi|$ in the opposite direction of the Sun's rigid rotation (the rigid rotation rate is $\Omega_\odot$). Footpoints also move in co-latitude at rate $\omega_\theta = |\omega_\theta|$.

We take the interface between fast and the rarefaction region tilted by angle Ψ with respect to the azimuthal direction. On the inner boundary surface, at radius R_B, the unit vector along the stream interface is defined

$$\hat{e}_I = \sin\Psi \hat{e}_\theta + \cos\Psi \hat{e}_\phi. \tag{A1}$$

On the inner boundary the unit vector normal to the stream interface is defined,

$$\hat{e}_\perp|_{r=R_B} = -\cos\Psi \hat{e}_\theta + \sin\Psi \hat{e}_\phi. \tag{A2}$$

Therefore the footpoint rotation rate normal to the stream interface is

$$\omega_\perp = -\omega_\theta \cos\Psi + \omega_\phi \sin\theta \sin\Psi. \tag{A3}$$

The footpoint rotation rate times the velocity gradient is

$$\alpha = R_B \boldsymbol{\omega}_B \cdot \nabla V|_{r=R_B} = \omega_\theta \frac{\partial V}{\partial \theta} + \omega_\phi \frac{\partial V}{\partial \phi} \tag{A4}$$

$$= R_B \omega_\perp \frac{\partial V}{\partial s_\perp} \tag{A5}$$

where the velocity gradient normal to the interface is

$$R_B \frac{\partial V}{\partial s_\perp} = \left(\omega_\theta \frac{\partial V}{\partial \theta} + \omega_\phi \frac{\partial V}{\partial \phi} \right) (\omega_\perp)^{-1}. \tag{A6}$$

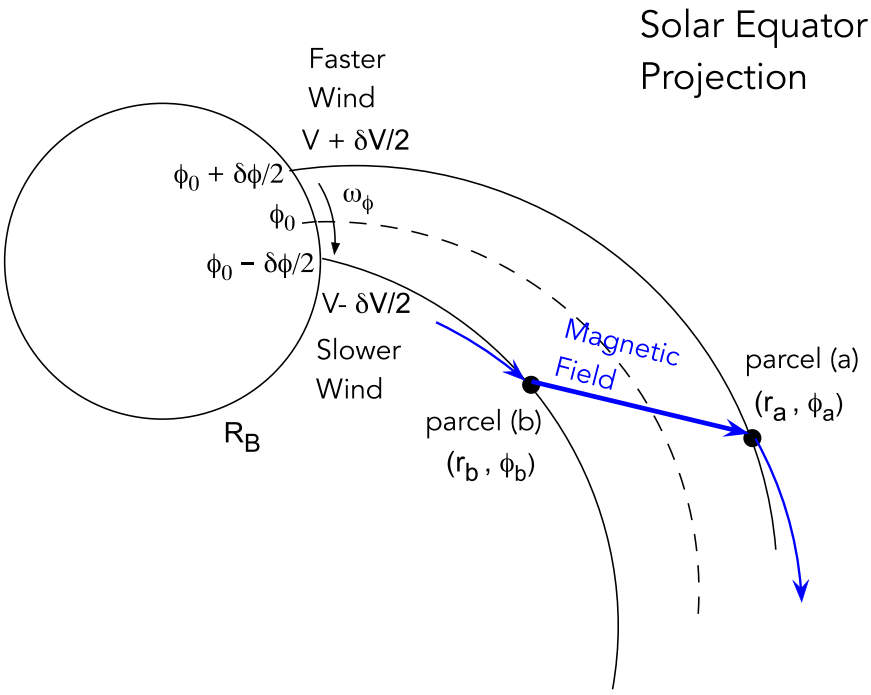

Figure 4. Footpoint motion across gradients in radial solar wind speed from faster into slower create the conditions for the sub-Parker spiral. Black-curves show the streamlines associated with parcel (a) and parcel (b) in the co-rotating reference frame. Footpoint motion provides a magnetic connection between parcel (a) and (b), which implies that the magnetic field is directed along the displacement between these plasma parcels. This projection is on the Sun's equatorial plane.

In the application to the rarefaction region considered here ω_ϕ is a negative quantity since longitudinal footpoint motion opposes solar rotation, and ω_θ is positive. This implies that $\omega_\perp < 0$,

$$\omega_\perp = -(\omega_\theta \cos\Psi + |\omega_\phi| \sin\theta \sin\Psi). \tag{A7}$$

The velocity gradient in co-latitude is a negative quantity, $\partial V/\partial\theta < 0$, and the velocity gradient in the azimuthal direction is a positive quantity, $\partial V/\partial\phi > 0$. Therefore, the velocity gradient normal to the interface is a positive quantity,

$$R_B \frac{\partial V}{\partial s_\perp} = \left(\omega_\theta \left| \frac{\partial V}{\partial \theta} \right| + |\omega_\phi| \frac{\partial V}{\partial \phi}\right) |\omega_\perp|^{-1} > 0. \tag{A8}$$

Given these properties of the velocity and footpoint rotation rates, Schwadron et al. (2020) expressed the magnetic field in the rarefaction region as follows

$$\boldsymbol{B} = A(\boldsymbol{r})\left\{\left(1 + |\alpha| \frac{(r - R_B)}{V^2}\right)\hat{e}_r - \frac{\boldsymbol{\omega}_B r}{V} - \frac{\Omega_\odot r \sin\theta}{V}\hat{e}_\phi\right\} \tag{A9}$$

where

$$\boldsymbol{\omega}_B = \omega_\theta \hat{e}_\theta + \omega_\phi \sin\theta \hat{e}_\phi, \tag{A10}$$

$$A(r) = B_{fB}\left(\frac{R_B}{r}\right)^2 \left(1 + \frac{|\alpha|}{|\omega_\perp|}\frac{(r - R_B)}{V^2}\Omega_\odot \sin\theta \sin\Psi\right)^{-1} \tag{A11}$$

and B_{fB} normalizes the magnetic field in the ambient fast solar wind. The corresponding magnetic field in the ambient fast solar wind is:

$$\boldsymbol{B}_f = B_{fB}\left(\frac{R_B}{r}\right)^2 \left(\hat{e}_r - \frac{\boldsymbol{\omega}_B r}{V} - \frac{\Omega_\odot r \sin\theta}{V}\hat{e}_\phi\right). \tag{A12}$$

A specific realization of the sub-Parker spiral with $\Psi = 0$ reveals the essence of the magnetic structure. In this case, the vector perpendicular to the stream interface is $\hat{e}_\perp = -\hat{e}_\theta$ and the sub-Parker magnetic field is given by

$$\boldsymbol{B}_a = B_{fB}\left(\frac{R_B}{r}\right)^2 \left\{\left(1 + \omega_\theta \left| \frac{\partial V}{\partial \theta} \right|_{r=R_B} \frac{(r - R_B)}{V^2}\right)\hat{e}_r - \frac{\boldsymbol{\omega}_B r}{V} - \frac{\Omega_\odot r \sin\theta}{V}\hat{e}_\phi\right\}. \tag{A13}$$

In this expression, for simplicity we have taken the solar wind speed as a function of latitude, with higher speed wind at higher latitudes and slower solar wind at lower latitudes. The expression in Equation (A13) can be generalized for any solar wind speed gradient, and any value of ω_θ:

$$\boldsymbol{B}_a = B_{fB}\left(\frac{R_B}{r}\right)^2 \left\{\left(1 - \omega_\theta \frac{\partial V}{\partial \theta} \Big|_{r=R_B} \frac{(r - R_B)}{V^2}\right)\hat{e}_r - \frac{\boldsymbol{\omega}_B r}{V} - \frac{\Omega_\odot r \sin\theta}{V}\hat{e}_\phi\right\}. \tag{A14}$$

In the case that $\omega_\theta \partial V/\partial\theta|_{r=R_B} < 0$, the expression conforms to the sub-Parker spiral solution. However, for $\omega_\theta \partial V/\partial\theta|_{r=R_B} > 0$, we arrive at a solution where the radial component of the magnetic field decreases with distance, and then reverses sign, leading to the formation of a switchbacked magnetic field. This is the solution for super-Parker spiral. With faster wind at higher latitudes, and slower wind at lower latitudes, the gradient $\partial V/\partial\theta|_{r=R_B} < 0$. As a result, the sign of ω_θ determines whether

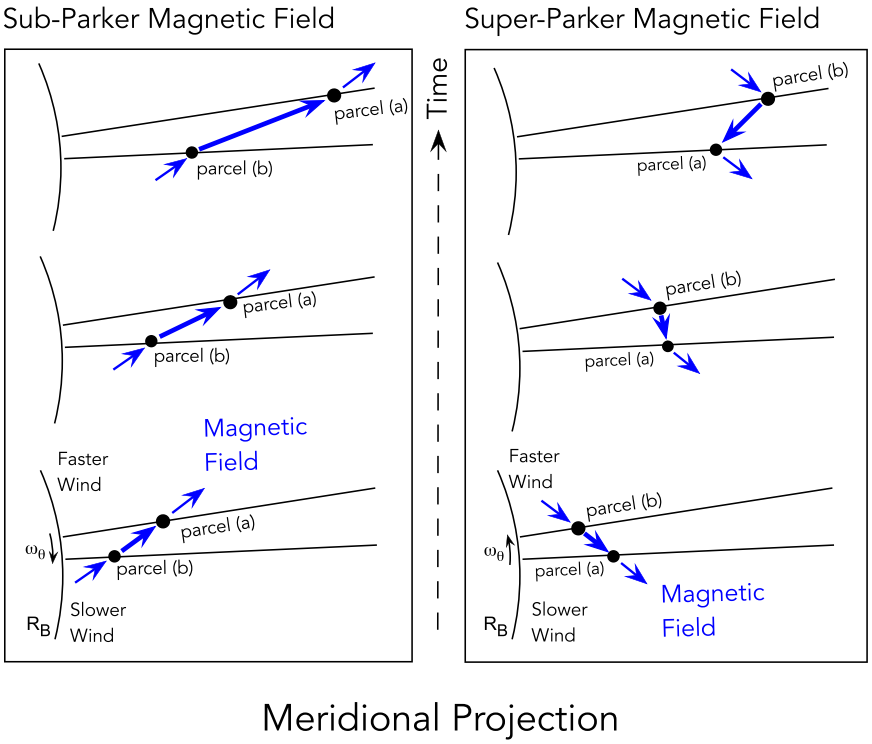

Figure 5. Comparison between the effects of footpoint motion from faster into slower solar wind in the case of the sub-Parker magnetic field (left panel) and from slower into faster solar wind in the case of the super-Parker magnetic field (right panel). Black-curves show the streamlines associated with parcel (a) released earlier and parcel (b) released later after footpoints have moved in latitude in the direction indicated. In the case (left panel) that footpoints move from the source of faster solar wind to slower wind, magnetic field lines are stretched in the radial direction forming the sub-Parker spiral. Note that a meridional projection is used in this figure, as opposed to the equatorial projection in Figure 4. Reversing the sense of the footpoint motion (right panel) leads to contraction of the magnetic field by the solar wind speed gradient, and ultimately leads to reversal of the field polarity associated with switchbacks.

the solution conforms to sub-Parker spiral ($\omega_\theta > 0$) or a super-Parker spiral ($\omega_\theta < 0$). Stated more generally: the sub-Parker spiral results when footpoints move from fast wind into slow wind ($\omega_\theta \partial V/\partial\theta|_{r=R_B} < 0$); the super-Parker spiral results when footpoints move from slow wind into fast wind ($\omega_\theta \partial V/\partial\theta|_{r=R_B} > 0$). Figure 5 shows a meridional projection for streamlines and the resulting magnetic field configuration in the case of a sub-Parker (left panel) and a super-Parker (right panel).

It is interesting to note that Equation (A14), which admits both sub-Parker and super-Parker solutions, requires a configuration where the solar wind speed is a function of latitude, as consistent with a latitudinal shear in the solar wind. In contrast, if speed variations exist such that faster wind trails slower wind in longitude, these structures must lead to the formation of compression regions, which complicate, or disallow steady-state solutions for the magnetic field structure. The treatment of latitudinal shear in the solar wind is similar and allows straightforward insight into the structural evolution of the magnetic field.

In the case of the super-Parker spiral, the switchbacked magnetic field appears at radial distances where

$$1 - |\omega_\theta| \left| \frac{\partial V}{\partial \theta} \right|_{r=R_B} \frac{(r - R_B)}{V^2} < 0, \qquad \text{(A15)}$$

or equivalently where

$$r > R_B + \frac{V^2}{|\omega_\theta||\partial V/\partial\theta|_{r=R_B}}. \qquad \text{(A16)}$$

As a specific example, if we consider an azimuthal motion of footpoints in the direction of solar rotation at 17% of the solar rotation rate, a radial distance of 0.3 au, a boundary surface at $R_B = 25$ solar radii, a speed change of 100 km s^{-1}, and an average wind speed of 300 km s^{-1}, then a switchback is created if the speed gradient exists over a displacement of $<0.^\circ 8$.

In Figure 6, we show the radial component of the magnetic field and its strength as a function of radial distance based on Equation (A14). For simplicity, we consider a specific instance where there is a speed change of 50 km s^{-1} across a region of $0.^\circ 1$ and an average wind speed of 400 km s^{-1}. Note that a $0.^\circ 1$ structure co-rotates past the a stationary observer in $\sim$10 minutes. The three cases shown are for the sub-Parker spiral (blue curve), the Parker spiral (black curve), and the super-Parker spiral (green). The only factor differentiating between these instances is the rate of footpoint motion. In the case of the Parker spiral, the footpoints are fixed and the rotation rate of footpoints is zero. For the sub-Parker spiral the footpoints rotate from the faster wind at higher latitudes into the slower wind at lower latitudes and the rate of footpoint motion is 10% of the solar rotation rate. For the super-Parker spiral, the footpoint motion is reversed, with footpoints moving from slower wind at lower latitudes into faster wind at higher latitudes, again at 10% of the solar rotation rate. In this case, the super-Parker spiral magnetic field reverses its radial component forming a switchback at 0.22 au.

The key features associated with the three field configurations are as follows:

1. the Parker spiral magnetic field has a radial component that drops as $\sim 1/r^2$ close to the Sun.

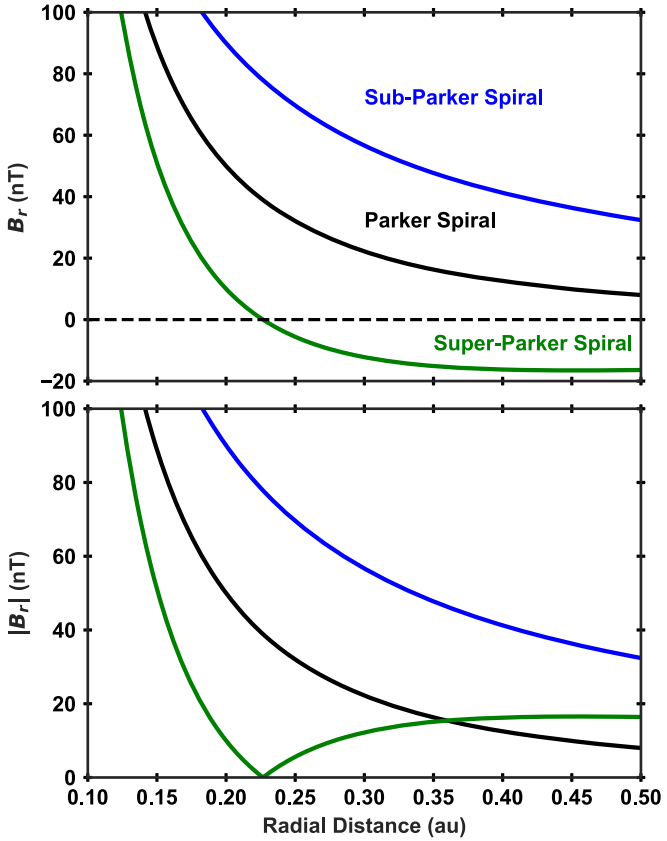

Figure 6. We use Equation (A14) to solve for the evolution of the magnetic field as a function of distance from the Sun for a Parker spiral with magnetic footpoints fixed in the co-rotating frame, a sub-Parker spiral with magnetic footpoints moving near the Sun from the source region of faster solar wind into the source of slower solar wind, and the super-Parker spiral with magnetic footpoints moving in the opposite direction from slower solar wind flow into faster solar wind flow.

2. the sub-Parker spiral magnetic field has a radial component that also drops as $\sim 1/r^2$ close to the Sun, but the radial component is significantly larger than that of the Parker spiral. This increase in radial magnetic field strength is counter-intuitive and results from the amplification of the radial component of the magnetic field as the field is stretched radially in between the faster and slower solar wind flow.
3. the super-Parker spiral initially has the weakest field strength and the weakest of radial component of the three magnetic configurations. The radial component of the field is reduced faster than the Parker spiral magnetic field, and ultimately reverses to form a switchback, in this case at $\sim$0.22 au. Beyond the switchback, the radial component of the field continues to drop with distance, and the magnitude of the radial magnetic field ultimately overtakes that of the Parker spiral magnetic field. This interesting increase in the radial field magnitude is also the result of the stretching of the reversed magnetic field between the faster and slower solar wind flow.

It is important to note that the sub-Parker spiral magnetic field can persist within the rarefaction region many au from the Sun, growing to fill an increasing volume of the inner heliosphere. In contrast, the super-Parker spiral is associated with compression between faster and slower solar wind flow. In the case considered, where the gradient in wind speed is across latitude, the faster and slower flows can continue to stretch the field. However, this idealization is unlikely to apply over broad regions, and eventually a compression region will form that slows the faster wind and speeds up the slower wind. This compression region will subsume the super-Parker spiral within the inherently turbulent flow within compression regions.

Another important feature associated with sub-Parker spiral and the super-Parker spiral is the specific alignment of flow deviations with the direction of the magnetic field. Generally, the non-radial magnetic field components will be directed opposite from the direction of footpoint motion. In the case considered with faster wind at higher latitude and slower wind at lower latitude, the non-radial field component will be directed with a positive latitudinal deviation for the sub-Parker spiral, and a negative latitudinal deviation for the super-Parker spiral. However, the faster flow will lead to compression of the plasma on the flux tube beneath the Alfvén surface, causing a density enhancement and non-radial flow deviation in the direction of the magnetic field. The super-Parker spiral will therefore have non-radial flow deviations that align with the magnetic field. In this context, the fact that PSP observes flows significantly larger than those in the Weber–Davis model (Kasper et al. 2019), and that the flow deviations are directed parallel to the magnetic field deviations is consistent with the super-Parker spiral. The compression side of fast-to-slow wind interface has slower wind leading faster wind in longitude, and the flow deviation is directed positively in longitude, in the same sense as co-rotation. As a result, near the source of the super-Parker spiral, we expect what would appear to be co-rotational flows to distances beyond the Alfvén critical point.

The sub-Parker spiral has faster wind leading slower wind. This will tend to reduce flow deviations and form rarefaction regions as these structures evolve with distance. These weaker flow deviations and reduced solar wind density within the rarefaction region provide distinct observational features that can differentiate regions that form the super-Parker spiral from those that form the sub-Parker spiral magnetic field.

ORCID iDs

N. A. Schwadron https://orcid.org/0000-0002-3737-9283
D. J. McComas https://orcid.org/0000-0001-6160-1158

References

Bale, S. D., Badman, S. T., Bonnell, J. W., et al. 2019, Natur, 576, 237
Bale, S. D., Goetz, K., Harvey, P. R., et al. 2016, SSRv, 204, 49
Balogh, A., Forsyth, R. J., Lucek, E. A., Horbury, T. S., & Smith, E. J. 1999, GeoRL, 26, 631
Bird, M. K., & Edenhofer, P. 1990, in Physics of the Inner Heliosphere, Vol. 1 ed. R. Schwenn & E. Marsch (Berlin: Springer)
Borovsky, J. E. 2016, JGRA, 121, 5055
Crooker, N. U., Gosling, J. T., & Kahler, S. W. 2002, JGRA, 107, 1028
de Wit, T. D., Krasnoselskikh, V. V., Bale, S. D., et al. 2020, ApJS, 246, 39
DeForest, C. E., Matthaeus, W. H., Viall, N. M., & Cranmer, S. R. 2016, ApJ, 828, 66
Fisk, L. A., & Kasper, J. C. 2020, ApJL, 894, L4
Fisk, L. A., & Schwadron, N. A. 2001, ApJ, 560, 425
Fisk, L. A., Zurbuchen, T. H., & Schwadron, N. A. 1999, ApJ, 521, 868
Fox, N. J., Velli, M. C., Bale, S. D., et al. 2016, SSRv, 204, 7
Goelzer, M. L., Schwadron, N. A., & Smith, C. W. 2014, JGRA, 119, 115
Gosling, J. T., & Skoug, R. M. 2002, JGR, 107, 1327
Gosling, J. T. 1975, RvGeo, 13, 1053
Gosling, J. T., Baker, D. N., Bame, S. J., Feldman, W. C., & Zwickl, R. D. 1987, JGR, 92, 8519
Gosling, J. T., McComas, D. J., Roberts, D. A., & Skoug, R. M. 2009, ApJL, 695, L213

Gosling, J. T., Tian, H., & Phan, T. D. 2011, ApJL, 737, L35
Horbury, T. S., Matteini, L., & Stansby, D. 2018, MNRAS, 478, 1980
Horbury, T. S., Woolley, T., Laker, R., et al. 2020, ApJS, 246, 45
Kahler, S. W., Crocker, N. U., & Gosling, J. T. 1996, JGRA, 101, 24373
Kasper, J. C., Abiad, R., Austin, G., et al. 2016, SSRv, 204, 131
Kasper, J. C., Bale, S. D., Belcher, J. W., et al. 2019, Natur, 576, 228
Katsikas, V., Exarhos, G., & Moussas, X. 2010, AdSpR, 46, 382
McComas, D. J. 1995, RvGeo, 33, 603
McComas, D. J., Alexander, N., Angold, N., et al. 2016, SSRv, 204, 187
McComas, D. J., Gosling, J. T., Phillips, J. L., et al. 1989, JGRA, 94, 6907
McComas, D. J., Gosling, J. T., & Phillips, J. L. 1992, JGR, 97, 171
McComas, D. J., Phillips, J. L., Hundhausen, A. J., & Burkepile, J. T. 1991, GeoRL, 18, 73
McComas, D. J., Velli, M., Lewis, W. S., et al. 2007, RvGeo, 45, RG1004
Michel, F. C. 1967, JGR, 72, 1917
Mozer, F. S., Agapitov, O. V., Bale, S. D., et al. 2020, ApJS, 246, 68
Murphy, N., Smith, E. J., & Schwadron, N. A. 2002, GeoRL, 29, 2066
Neugebauer, M., & Goldstein, B. E. 2013, in AIP Conf. Proc. 1539, Solar Wind, ed. G. P. Zank et al. (Melville, NY: AIP), 46
Poletto, G. 2015, LRSP, 12, 7
Rouillard, A. P., Kouloumvakos, A., Vourlidas, A., et al. 2020, ApJS, 246, 37
Ruffolo, D., Matthaeus, W. H., Chhiber, R., et al. 2020, ApJ, 902, 94
Schatten, K. H., Wilcox, J. M., & Ness, N. F. 1969, SoPh, 6, 442
Schwadron, N. A. 2002, GeoRL, 29, 1663
Schwadron, N. A., Joyce, C. J., Aly, A., et al. 2020, A&A, in press
Schwadron, N. A., & McComas, D. J. 2003, AdSpR, 32, 531
Schwadron, N. A., & McComas, D. J. 2005, GeoRL, 32, L03112
Schwadron, N. A., McComas, D. J., Elliott, H. A., et al. 2005, JGRA, 110, A04104
Schwenn, R. 1990, in Physics of the Inner Heliosphere, Vol. 1 ed. R. Schwenn & E. Marsch (Berlin: Springer), 99
Smith, E. J., Balogh, A., Forsyth, R. F., Tsurutani, B. T., & Lepping, R. P. 2000, AdSpR, 26, 823
Snodgrass, H. B. 1983, ApJ, 270, 228
Tenerani, A., Velli, M., Matteini, L., et al. 2020, ApJS, 246, 32
Weber, E. J., & Davis, L., Jr. 1967, ApJ, 148, 217
Yamauchi, Y., Moore, R. L., Suess, S. T., Wang, H., & Sakurai, T. 2004a, ApJ, 605, 511
Yamauchi, Y., Suess, S. T., Steinberg, J. T., & Sakurai, T. 2004b, JGRA, 109, A03104
Zank, G. P., Nakanotani, M., Zhao, L.-L., Adhikari, L., & Kasper, J. 2020, ApJ, 903, 1